World Electric Vehicle Journal

MDPI

Article

Research on Vertical Parking Path Planning Based on Circular Arcs, Straight Lines, and Multi-Objective Evaluation Function

Junpeng Ma and Yubin Qian *

School of Mechanical and Automotive Engineering, Shanghai University of Engineering Science, Shanghai 201620, China; majunpeng0313@163.com
* Correspondence: qianyb@sues.edu.cn

Abstract: In the vertical parking process, the issue of turning in place due to discontinuities in path curvature is addressed by proposing an optimal reference path planning method based on circular arcs, straight lines, and a multi-objective evaluation function. This method first analyzes the obstacle avoidance constraints between the vehicle's outer contour and the parking space, as well as the vehicle's kinematic constraints. The feasible driving region's upper and lower boundaries are determined by tangent circular arcs and straight lines. Subsequently, a multi-objective evaluation function is designed, which integrates path curvature, adjustable margins at any given moment, and path length, to obtain the optimal circular arc and straight line combination within the feasible region. Finally, the path is fitted using a polynomial curve to form the optimal reference path. Simulation results demonstrate that the planned path satisfies both the continuity of path curvature and the vehicle's kinematic constraints.

Keywords: vertical parking; path planning; circular arc–line tangency; multi-objective optimization

check for updates

Academic Editors: Liguo Zang and Leilei Zhao

Received: 6 February 2025
Revised: 28 February 2025
Accepted: 3 March 2025
Published: 5 March 2025

Citation: Ma, J.; Qian, Y. Research on Vertical Parking Path Planning Based on Circular Arcs, Straight Lines, and Multi-Objective Evaluation Function. *World Electr. Veh. J.* **2025**, *16*, 152. https://doi.org/10.3390/wevj16030152

Copyright: © 2025 by the authors. Published by MDPI on behalf of the World Electric Vehicle Association. Licensee MDPI, Basel, Switzerland. This article is an open access article distributed under the terms and conditions of the Creative Commons Attribution (CC BY) license (https://creativecommons.org/licenses/by/4.0/).

1. Introduction

In recent years, with the continuous improvement in the national economy, the automotive industry has developed rapidly, leading to a sharp increase in the number of vehicles and resulting in increasingly severe issues such as traffic congestion, limited parking spaces, and the difficulty of finding parking. To effectively address these problems, automatic parking technology has emerged and gradually become a key technical means to solve them [1]. Currently, automatic parking technology mainly consists of three key components: environmental perception, path planning, and tracking control [2]. Among these, the primary goal of path planning is to devise a collision-free path that complies with the vehicle's dynamic constraints based on the vehicle's current position and the target parking space in specific parking scenarios. As one of the core technologies of automatic parking systems, the quality of path planning directly affects the overall performance of the system. Therefore, researching parking path planning algorithms that adapt to complex environments holds significant practical importance and broad application value.

As a critical component of intelligent driving technology, automated parking systems rely on three core technologies: environmental perception, path planning, and trajectory tracking control [3]. Among these, path planning plays a pivotal role in determining the performance of the system, directly influencing the smoothness and efficiency of the parking process [4,5]. Despite the availability of various path planning methods, technical difficulties remain in practical applications. For instance, paths generated by traditional geometric

methods often exhibit curvature discontinuities at transitions between arcs and straight lines, necessitating in-place steering adjustments that compromise vehicle maneuverability and ride comfort [6–9]. Although introducing straight segments or clothoid curves alleviates this issue to some extent [10,11], such methods are highly dependent on the initial vehicle pose, limiting their adaptability across scenarios. On the other hand, numerical optimization methods can generate curvature-continuous paths by constructing multi-objective optimization models, effectively optimizing path time or length [12–15], but their high computational complexity makes real-time application challenging. Sampling-based approaches, such as the RRT algorithm, enhance adaptability to complex scenarios by randomly sampling in free space and constructing a path graph [16,17]. However, they suffer from poor path smoothness and long computation times. Machine learning-based strategies, particularly those leveraging imitation learning or reinforcement learning, improve generalizability in path planning [18–23], but the performance gap between simulation environments and real-world applications still needs to be addressed.

To address these challenges, researchers worldwide have proposed several improved methods in recent years. For example, Ref. [8] proposed a planning method based on tangential arcs and straight lines, which is computationally simple but still suffers from curvature discontinuities. The study in [13] developed a multi-objective optimization model to generate optimal parking paths with improved smoothness. Reference [24] combined sampling methods with nonlinear optimization algorithms, enhancing adaptability across various parking scenarios. Moreover, Ref. [23] applied reinforcement learning techniques, using nonlinear programming to generate training data and optimize policy networks, thereby improving system generalization. As shown in Table 1, a comparison of automated parking path planning methods reveals the strengths and limitations of various approaches.

Table 1. Comparison of automated parking path planning methods.

Method	Computation Time	Smoothness	Scene Adaptability	Number of Turns
geometric method	very short	good	poor	moderate
numerical optimization	very long	good	good	few
graph search	moderate	poor	good	many
sampling method	moderate	moderate	moderate	few

To address these limitations, this study proposes a vertical parking path planning method that combines circular arcs, straight lines, and a multi-objective optimization function. From a broader market perspective, this approach holds significant potential for integration into real-world autonomous parking systems, particularly in vehicles with advanced parking technologies. As autonomous vehicles continue to gain traction, the adoption of this method in vehicle systems may lead to notable improvements in parking efficiency and safety. Additionally, future advancements, such as the incorporation of rear-wheel steering or advanced obstacle detection systems, could further enhance the performance and effectiveness of the proposed method.

2. Vehicle Modeling and Parking Scene Construction

2.1. Kinematic Modeling of the Vehicle

In the parking process, the vehicle typically operates at speeds below 5 km/h, where lateral sliding of the wheels is generally negligible. For simplicity, the wheels are assumed to perform only rolling and steering motions, and the vehicle is modeled as a rigid body [25]. This assumption neglects factors such as tire deformation and frictional forces that might affect the vehicle's motion in real-world conditions. Based on the Ackermann steering

principle, a kinematic model of the vehicle was constructed, as shown in Figure 1. While this simplified model is useful for path planning in controlled environments, it may not fully account for the complexities of vehicle dynamics in more challenging parking scenarios, such as those involving steep slopes or low-traction surfaces.

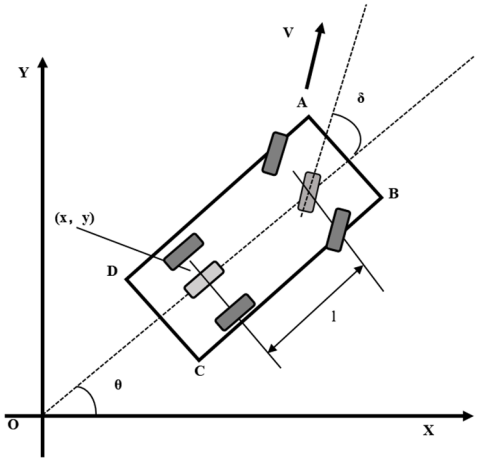


Figure 1. Vehicle kinematic model.

The vehicle kinematic equations presented in this paper are as follows:

$$\begin{cases} \dot{x}_r = v cos\theta \\ \dot{y}_r = v sin\theta \\ \dot{\theta} = \frac{v tan\varphi}{l} \end{cases}, \tag{1}$$

In the equation, l represents the vehicle's wheelbase, θ denotes the vehicle's heading angle, (x_f, y_f) represents the coordinates of the front axle center, (x_r, y_r) represents the coordinates of the rear axle center, φ is the vehicle's equivalent front wheel steering angle, v_f represents the velocity at the front axle center, and v_r represents the velocity at the rear axle center. When the vehicle is driving with the minimum turning radius, the minimum turning radius R_{r}, the maximum steering angle δ_{max} of the front wheels, and the minimum turning radius R_{min} at the rear axle center satisfy the following relationship:

$$\begin{cases} R_{min} = \sqrt{R_r^2 - l^2} - 0.5w \\ tan\delta_{min} = \frac{l}{R_{min}} \end{cases}, \tag{2}$$

In autonomous parking research, the vehicle's motion state is primarily represented by the coordinates (x_r, y_r) of the rear axle center in the coordinate system, as well as the heading angle θ. In path planning, to ensure that the vehicle does not collide with obstacles in the parking environment during the path planning process, it is also necessary to describe the motion of the vehicle's body outline. By combining the vehicle's front overhang length l_f, rear overhang length l_r, and vehicle width w, the coordinates of the four vertices A, B, C, and D can be obtained as follows:

The front-left vertex A of the vehicle:

$$\begin{cases} x_A = x_r + \left(l + l_f\right) cos\theta - \frac{w}{2} sin\theta \\ y_A = y_r + \left(l + l_f\right) sin\theta + \frac{w}{2} cos\theta \end{cases}, \tag{3}$$

The front-right vertex B of the vehicle:

$$\begin{cases} x_B = x_r + \left(l + l_f\right)cos\theta + \frac{w}{2}sin\theta \\ y_B = y_r + \left(l + l_f\right)sin\theta - \frac{w}{2}cos\theta \end{cases}' \tag{4}$$

The rear-right vertex C of the vehicle:

$$\begin{cases} x_C = x_r - l_r cos\theta + \frac{w}{2}sin\theta \\ y_C = y_r - l_r sin\theta - \frac{w}{2}cos\theta \end{cases}' \tag{5}$$

The rear-left vertex D of the vehicle:

$$\begin{cases} x_D = x_r - l_r cos\theta - \frac{w}{2}sin\theta \\ y_D = y_r - l_r sin\theta + \frac{w}{2}cos\theta \end{cases}' \tag{6}$$

2.2. Parking Scene Setting

This study primarily focuses on vertical parking spaces, and its simplified model is shown in Figure 2. The direction perpendicular to the parking space is defined as the X-axis, while the direction parallel to the parking space is defined as the Y-axis, establishing the global coordinate system for vertical parking. Considering the generality of the path planning algorithm, according to the ISO 16787 standard [26], for test vehicles with a length of 4 m or less, the parking space length L is equal to the length of the test vehicle l_c, and the parking space width w_q is the width of the test vehicle W plus 1.2 m. The road width H is 4.5 m. The relevant parameters are shown in Table 2.

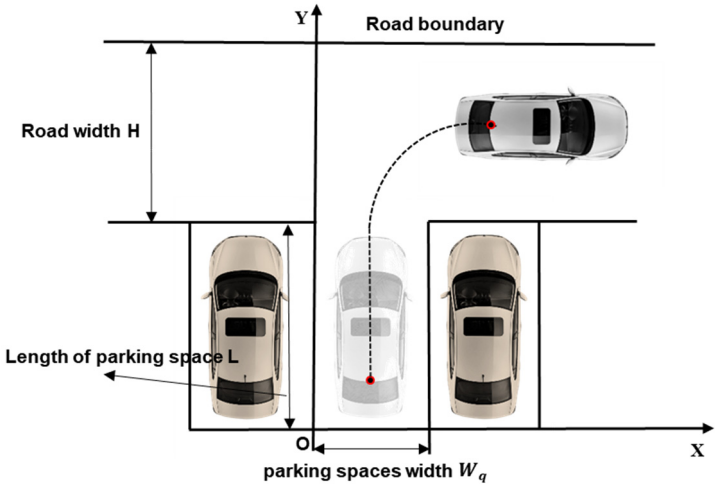


Figure 2. Simplified model of a vertical parking space.

Table 2. Vertical parking space dimensions.

Parameters	Numerical Value
length of parking space L/m	l_c
body width W/m	W + 1.2
road width H/m	4.5

The proposed path planning method assumes a flat parking space. However, in real-world scenarios, parking areas may feature varying slopes and curvatures that can significantly influence the vehicle's trajectory. These topological parameters are not considered in the current study, but future research will investigate how to integrate these

factors into the model. By incorporating slope and curvature variations, we aim to enhance the robustness and applicability of the path planning method in complex parking environments.

In real-world vertical parking scenarios, parking space topography, including slope and curvature, plays a critical role in the vehicle's path planning. For instance, when the parking area has an incline, the vehicle's dynamics, such as its ability to steer and its trajectory, may be altered. Similarly, the curvature of the parking space can affect the optimal path design, necessitating adjustments to the planned trajectory to accommodate these variations. The current study does not account for these variations but recognizes the need for further exploration in future research to improve the generalizability and performance of the proposed method. Incorporating topological factors into the model would increase the method's practical applicability, ensuring it performs effectively in a wider range of real-world parking environments.

3. Research on Vertical Parking Path Planning

Geometric planning methods offer advantages in computational efficiency and real-time performance, particularly when using the arc–line tangent method, which can plan the shortest path. In contrast, numerical optimization methods are unconstrained by the vehicle's initial parking pose and have strong scene adaptability. Therefore, this research combines the advantages of both geometric and numerical optimization methods and proposes a path planning approach based on arc–line and multi-objective evaluation functions.

As shown in Figure 3, when the parking starting point p_1 is known, the feasible region of the vertical parking path can be calculated using the following conditions: As shown in Figure 3a, the rear-left point $D^{'}$ of the vehicle does not collide with the left boundary of the parking space; as shown in Figure 3b, the right side of the vehicle does not collide with the right corner of the parking space; and as shown in Figure 3c, the front-left point $A^{'}$ of the vehicle does not collide with the upper boundary of the parking space.

Based on these conditions, the arc radii of the upper and lower boundaries of the feasible vertical parking region, R^{u}_{1max} and R^{l}_{1min}, as well as the coordinates of the intersection points of the arc and the line, p^{u}_{2} and p^{l}_{2}, can be determined, thereby defining the feasible parking path region, as shown in Figure 3d.

3.1. Determination of the Feasible Region for Vertical Parking

In vertical parking path planning, the determination of the feasible driving region is critical. This study approaches the analysis from the perspectives of the lower and upper boundaries, examining the constraints of the feasible region based on the geometric relationships of the vehicle.

3.1.1. Determination of the Lower Boundary

First, the lower bound of the feasible driving region for vertical parking is determined. As shown in Figure 4, when the vehicle moves along a smaller arc from the parking starting point, the right side of the vehicle is likely to collide with the upper-right corner A of the parking space. To avoid this collision and maintain a safe distance at point A, the first limiting value of the lower bound arc radius can be calculated based on geometric relationships.

$$\left(R^{l}_{1min1} - y_{p_1} + L\right)^2 + \left(X_{p_1} - w_q + l_1\right)^2 = \left(R^{l}_{1min1} - \frac{w}{2}\right)^2, \tag{7}$$

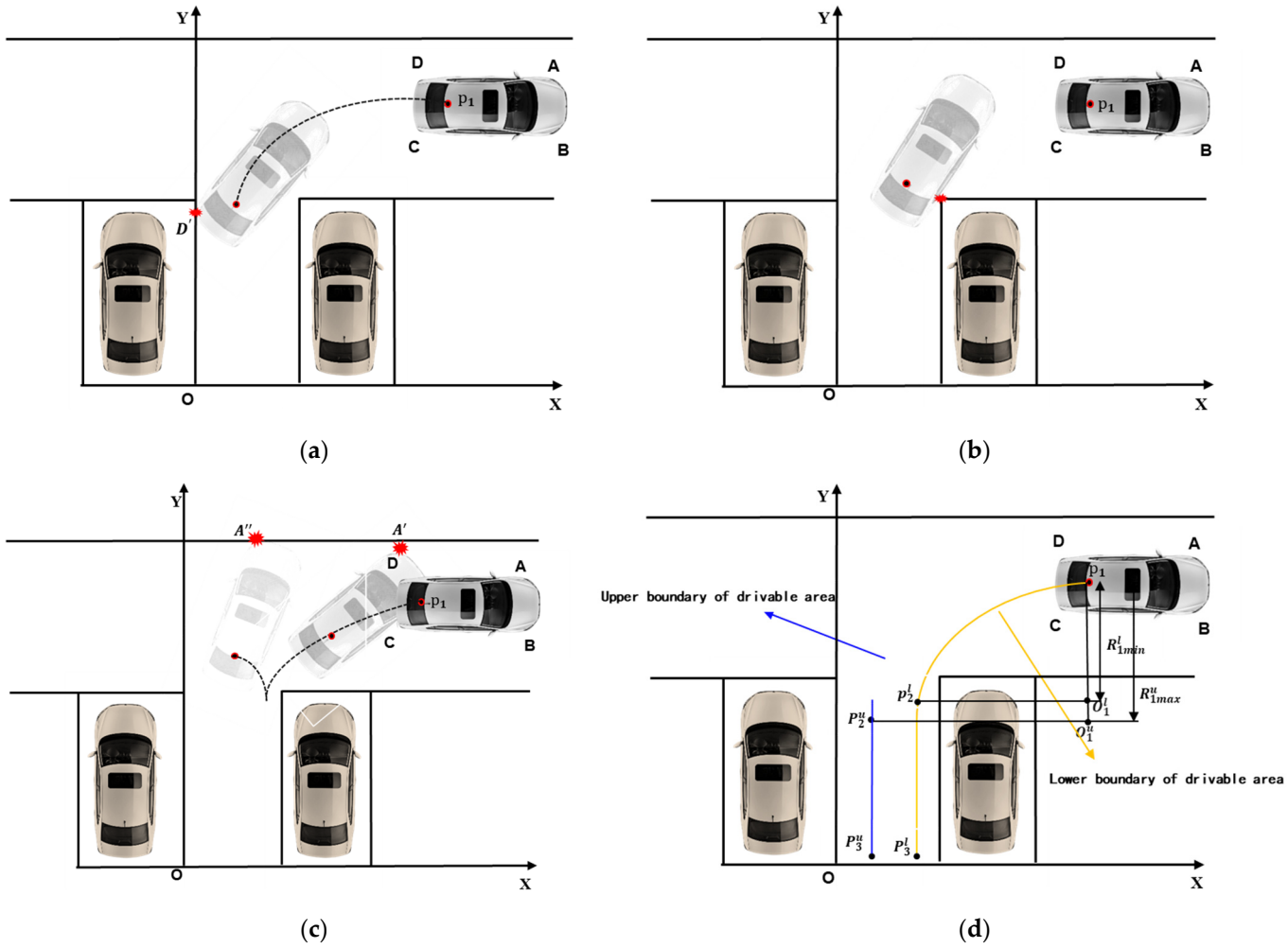


Figure 3. (**a**) Schematic of left boundary collision; (**b**) schematic of right boundary collision; (**c**) schematic of upper parking boundary collision; (**d**) schematic of the feasible region for vertical parking.

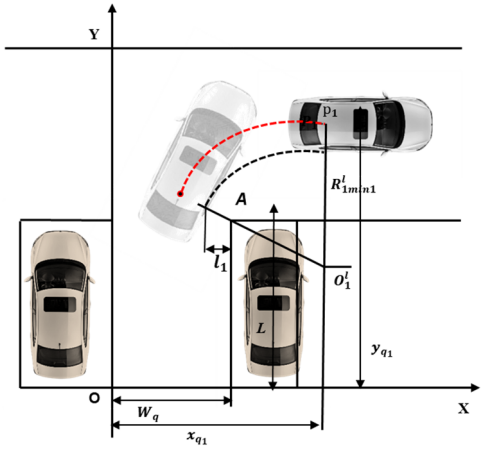


Figure 4. Analysis of the first limit value of the radius of the arc of the lower boundary of the vertical parking feasible region R^l_{1min1}. In the path planning process, the vehicle's pose is defined based on the coordinates of the rear axle center point, the red dash line represents the motion trajectory of the rear axle center point.

As shown in Figure 5, when the vehicle plans a path along a smaller arc from the parking starting point $p_1(x_{p_1}, y_{p_1})$, it is also necessary to consider potential collisions with the road boundary. Since the front-left point A of the vehicle is the first to contact the

road boundary, in order to avoid a collision and maintain a safety distance l_2 at the road boundary, the second limiting value of the lower boundary arc radius of the feasible vertical parking region, R^l_{1min2}, can be calculated based on geometric relationships.

$$\left(R^l_{1min2} + \frac{w}{2}\right)^2 + \left(l + l_f\right)^2 = \left(L - y_{p_1} + R^l_{1min2} + H + l_2\right)^2, \tag{8}$$

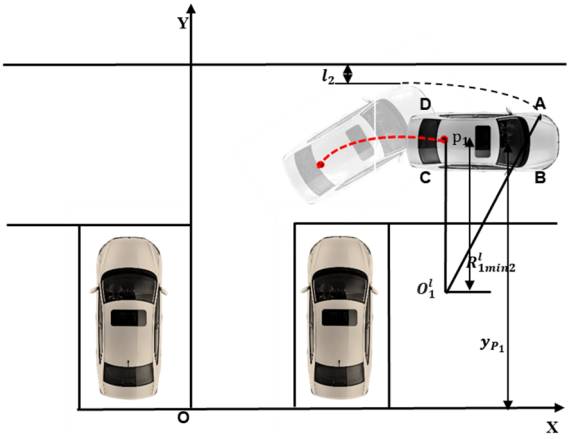


Figure 5. Analysis of the second limit value of the radius of the arc of the lower boundary of the vertically parked drivable area R^l_{1min2}. In the path planning process, the vehicle's pose is defined based on the coordinates of the rear axle center point, the red dash line represents the motion trajectory of the rear axle center point.

In vertical parking path planning, the vehicle's structural limitations must also be considered. Based on the two limiting values of the lower boundary arc radius of the feasible vertical parking region, the results should be compared with the minimum turning radius R_{min} of the vehicle's rear axle center. The minimum value among the three should be selected as the lower boundary arc radius R^l_{1min} of the feasible vertical parking region.

$$R^l_{1min} = \left\{R^l_{1min1}, R^l_{1min2}, R_{min}\right\}, \tag{9}$$

Based on the calculated lower boundary arc radius of the feasible vertical parking region, and considering that the vehicle should be parallel to the parking space's length direction at the parking endpoint, the straight line equation of the lower boundary of the feasible vertical parking region can be derived using the geometric relationship of the arc–line tangency. The equation is given by $x_1 = x_{P_1} - R^l_{1min}$.

3.1.2. Determination of the Upper Boundary

For the upper boundary of the feasible driving region in vertical parking, as shown in Figure 6, when the vehicle follows a larger circular arc path starting from the parking point $p_1(x_{p_1}, y_{p_1})$, the left rear point D of the vehicle reaches its maximum trajectory, making it prone to collision with the left boundary line of the parking space. To avoid such a collision and to maintain a safety margin l_3 from the left boundary line, the upper boundary circular arc radius R^u_{1max} can be calculated.

$$\left(X_{p_1} - l_3\right)^2 = \left(R^u_{1max} + \frac{w}{2}\right)^2 + l_r^2, \tag{10}$$

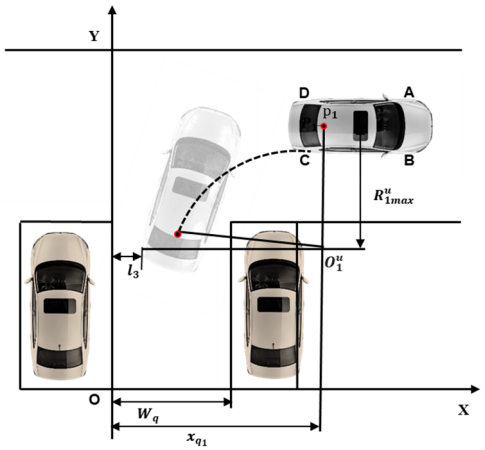


Figure 6. Vertical parking drivable area upper boundary arc radius R^u_{1max} analysis.

Similarly, based on the geometric relationship of tangency between the circular arc and the straight line, the equation of the upper boundary straight line can be expressed as $x_2 = X_{p_1} - R^u_{1max}$.

3.2. Design of Multi-Objective Evaluation Function for Vertical Parking

After determining the upper and lower boundaries of the drivable region, theoretically, any combination of circular arcs and straight lines within the region can satisfy the requirements of parking path planning. However, to further optimize parking performance, it is necessary to comprehensively consider factors such as path curvature smoothness, adjustable margin, and path length. Therefore, this study designed a multi-objective evaluation function to optimize and solve for the optimal combination of circular arcs and straight lines within the drivable region.

3.2.1. Path Curvature Smoothness

In vertical parking, avoiding large steering angles requires the path curvature to be as smooth as possible. Path curvature represents the degree of bending along the vehicle's travel path; the smaller the curvature, the smoother the path. To compute the path curvature, the vehicle's motion along the circular arc segments and straight segments must be considered. The curvature of the circular arc segments is determined by the radius R_i of the arc, and the curvature k_i can be expressed as the reciprocal of the radius:

$$k_i = \frac{1}{R_i}, \tag{11}$$

where R_i is the radius of the circular arc. A larger curvature indicates a sharper arc, while a smaller curvature corresponds to a smoother arc.

For the straight segments, the curvature is zero because straight lines do not bend:

$$k_i = 0, \tag{12}$$

The total curvature of the path is determined by the weighted average of the curvature in the circular arc and straight line segments. Assuming the vehicle starts at $p_1(x_{p_1}, y_{p_1})$, travels along a circular arc to point $p_2(x_{p_2}, y_{p_2})$, and then proceeds along a straight line to the endpoint $p_3(x_{p_3}, y_{p_3})$; the path curvature k_i can be expressed as follows:

$$k_i = \begin{cases} \frac{1}{R_i} & \left(x_{p_1} < x \ll x_{p_2}\right) \\ 0 & \left(x_{p_2} < x \ll x_{p_3}\right) \end{cases}, \tag{13}$$

To ensure the smoothness of the path curvature, upper and lower bounds for the curvature are defined. The maximum curvature occurs when the arc radius is at its minimum, and the minimum curvature occurs when the arc radius is at its maximum, specifically the following:

$$k_{min} = \frac{1}{R_{max}}, k_{max} = \frac{1}{R_{min}}, \tag{14}$$

The constraint for the path curvature k_i is given by the following:

$$k_{min} \ll k_i \ll k_{max}, \tag{15}$$

3.2.2. Maximizing Adjustability at Any Time

To ensure that the vehicle can flexibly adjust its trajectory during parking, the range of the front wheel steering angle α_{i} needs to be maximized. To maximize the steering angle margin, the following aspects must be considered:

1. Limit Steering Angles: The minimum and maximum values of the steering angle α_{i} correspond to the maximum and minimum values of the turning radius, respectively. When R_{i} takes its maximum value, the steering angle α_{i} reaches its minimum:

$$\alpha_{\min} = \arctan\left(\frac{\mathrm{L}}{R_{\max}}\right), \tag{16}$$

When R_{i} takes its minimum value, the steering angle α_{i} reaches its maximum:

$$\alpha_{\max} = \arctan\left(\frac{\mathrm{L}}{R_{\min}}\right), \tag{17}$$

2. Margin Optimization: To maximize the steering angle margin, an appropriate turning radius R_{i} must be selected during the path planning process, such that the following is satisfied:

$$\alpha_{\min} \ll \alpha_{\mathrm{i}} \ll \alpha_{\max}, \tag{18}$$

By discretizing and optimizing the turning radius, the radius value that provides the maximum adjustable margin can be selected.

3.2.3. Shortest Path Length

In vertical parking path planning, minimizing the path length aims to ensure that the vehicle completes the parking maneuver in the shortest possible distance, thereby reducing parking time and energy consumption. The total path length sis_isi can be expressed as the integral of the curve length of the planned path:

$$s_i = \int_{x_{p_1}}^{x_{p_3}} \sqrt{1 + y^2} dx, \tag{19}$$

The vertical parking path consists of a circular arc segment and a straight line segment, so the path length needs to be calculated separately for each part.

1. Arc Segment Length: The length of the arc segment can be calculated using the arc length formula. Assuming the arc radius is R_{i} and the central angle is θ_i, the length of the arc s_{arc} is the following:

$$s_{arc} = R_{\mathrm{i}} \cdot \theta_i, \tag{20}$$

where R_{i} is the radius of the circular arc, and θ_i is the central angle of the arc.

2. Line Segment Length: The length of the line segment can be calculated using the distance formula between two points. Assuming the coordinates of the start and

endpoints of the line segment are $p_2(x_{p_2}, y_{p_2})$, and $p_3(x_{p_3}, y_{p_3})$, the length of the line segment s_{line} is as follows:

$$s_{line} = \sqrt{\left(x_{p_3} - x_{p_2}\right)^2 + \left(y_{p_3} - y_{p_2}\right)^2}, \tag{21}$$

The total path length s_i is the sum of the arc length and the line segment length:

$$s_i = s_{arc} + s_{line}, \tag{22}$$

3.2.4. Design of the Evaluation Function

Based on the previous analysis, it is evident that when the path length is minimized, the path curvature is not smooth, and the adjustable margin at any moment is not maximized. These three factors are in conflict with each other. Therefore, an evaluation function is designed to calculate the trade-off between these metrics. The evaluation function is defined as follows:

$$E = a_1 \frac{k_i - k_{min}}{k_{max} - k_{min}} + a_2 \frac{\alpha_i - \alpha_{min}}{\alpha_{max} - \alpha_{min}} + a_3 \frac{s_i - s_{min}}{s_{max} - s_{min}}, \tag{23}$$

where a_1, a_2, a_3 are weight coefficients used to adjust the importance of each metric in the evaluation function; kik_iki represents the path curvature; α_i denotes the front wheel steering margin; and s_i is the path length. The standardization of each metric is as follows:

- $\frac{k_i - k_{min}}{k_{max} - k_{min}}$ is the normalized value of the path curvature;
- $\frac{\alpha_i - \alpha_{min}}{\alpha_{max} - \alpha_{min}}$ is the normalized value of the front wheel steering margin;
- $\frac{s_i - s_{min}}{s_{max} - s_{min}}$ is the normalized value of the path length.

To ensure the rationality of the computation, the following constraints are applied: the path curvature K is in the range $k_{min} \ll k_i \ll k_{max}$; the front wheel steering margin α is in the range $\alpha_{min} \ll \alpha_i \ll \alpha_{max}$; and the path length s is in the range $s_{min} \ll s_i \ll s_{max}$.

The optimization objective is to minimize the evaluation function E, thus balancing the path length, path curvature, and front wheel steering margin.

Explanation of Weight Coefficients Selection:

In this study, the weight coefficients in the evaluation function were chosen based on the actual demands of vehicle dynamics and path planning. The specifics are as follows: (1) Path Curvature: A higher weight was assigned to the path curvature term to ensure smoothness and vehicle controllability during the parking process. Smooth steering is particularly important in parking scenarios to avoid sharp turns that could compromise vehicle handling. This higher weight reduces the possibility of sharp curvature, which would require excessive steering adjustments, thereby enhancing both the comfort and safety of the parking maneuver. (2) Path Length: A moderate weight was given to the path length term with the objective of minimizing the distance the vehicle travels during parking. Minimizing the path length is essential for improving parking efficiency, reducing parking time, and optimizing space usage in confined parking areas. Given that parking spaces are often limited, this aspect of the evaluation function is crucial to ensure the most efficient use of available space. (3) Adjustable Margin: A moderate weight was assigned to the adjustable margin term. This margin ensures that the vehicle can make necessary adjustments during the parking process to avoid collisions with obstacles or the parking space boundaries. A higher weight on the adjustable margin would allow the vehicle to have more flexibility in adjusting its trajectory, improving the system's robustness.

3.3. Smoothing of Vertical Parking Paths

To avoid in-place steering phenomena in vertical parking path planning, it is necessary to ensure the continuity of path curvature. Curvature continuity requires that the second derivative of the path curve is continuous. Moreover, since the front wheel steering angle serves as the output of the control system and cannot exhibit abrupt changes during parking, the curve type must also ensure the continuity of the third derivative.

Considering that paths generated by the tangential method of arcs and straight lines generally exhibit a "C"-shaped pattern, this study employs a quartic polynomial to smooth the parking path. The expression for the quartic polynomial is given as follows:

$$y = b_0 + b_1 x + b_2 x^2 + b_3 x^3 + b_4 x^4, \tag{24}$$

The coefficients $b_0 - b_4$ of the quartic polynomial can be determined using the known points: the parking start point $p_1(x_{p_1}, y_{p_1})$, the parking endpoint $p_3(x_{p_3}, y_{p_3})$, and the intersection point $p_2(x_{p_2}, y_{p_2})$ between the arc and the straight line. The specific solution process is as follows:

To ensure that the vehicle's orientation at the parking endpoint is perpendicular to the parking space, the slope of the path at the endpoint must approach infinity. To simplify the calculations, the global coordinate system is rotated counterclockwise by 45°. The transformed coordinate system is represented as follows:

$$\begin{cases} X^T = Xcos45 - Ysin45 \\ Y^T = Xsin45 + Ycos45 \end{cases}, \tag{25}$$

To ensure that the path passes through both the parking start and endpoint coordinates, the following constraints are applied:

$$\begin{cases} y_{P_1} = b_0 + b_1 x_{p_1} + b_2 x_{p_1}^2 + b_3 x_{p_1}^3 + b_4 x_{p_1}^4 \\ y_{P_3} = b_0 + b_1 x_{p_3} + b_2 x_{p_3}^2 + b_3 x_{p_3}^3 + b_4 x_{p_3}^4 \end{cases}, \tag{26}$$

To ensure that the vehicle is parallel to the parking space at the starting point and perpendicular at the endpoint, the slope of the quartic polynomial must satisfy the following conditions:

$$\begin{cases} 1 = b_1 + 2b_2 x_{p_1} + 3b_3 x_{p_1}^2 + 4b_4 x_{p_1}^3 \\ -1 = b_1 + 2b_2 x_{p_3} + 3b_3 x_{p_3}^2 + 4b_4 x_{p_3}^3 \end{cases}, \tag{27}$$

To ensure obstacle avoidance, the path must pass through the intersection point $p_2(x_{p_2}, y_{p_2})$ of the arc and the straight line. The corresponding constraint is as follows:

$$y_{P_2} = b_0 + b_1 x_{p_2} + b_2 x_{p_2}^2 + b_3 x_{p_2}^3 + b_4 x_{p_2}^4, \tag{28}$$

Ultimately, by optimizing this evaluation function, the optimal combination of circular and straight paths within the drivable area is determined to achieve efficient and accurate vertical parking path planning.

4. Simulation Verification of Vertical Parking Path Planning

To validate the effectiveness of the proposed path planning method in vertical parking scenarios, this section presents a verification using the MATLAB R2020b simulation platform, with comparisons made to traditional geometric methods and numerical optimization methods. The experimental results demonstrate that the proposed method shows

significant advantages in terms of path planning accuracy, computational efficiency, and curvature smoothness.

4.1. Determination of the Feasible Region for Vertical Parking

The simulation scene is designed based on the standard "Performance Requirements and Testing Methods for Intelligent Parking Assist Systems" (GB/T 41630-2022) [27], selecting the geometric characteristics of a typical small car. The specific parameters are as follows: vehicle length is 2 m, width is 1.4 m, and wheelbase is 2.8 m; parking space length is 5 m and width is set to 3 m; road width is 4.5 m, with a safety margin of 0.05 m reserved; the minimum turning radius is 1.8 m.

In the design of the multi-objective evaluation function, the following indicators are considered: adjustable margin ($K_1 = 0.5$) reflecting the vehicle's ability to correct deviations from the expected trajectory; path curvature ($K_2 = 0.3$) indicating the comfort of vehicle control; and path length ($K_3 = 0.2$) impacting the economic efficiency of parking.

4.2. Simulation Experiment and Comparative Analysis

By setting weight coefficients to balance safety, comfort, and economy, the proposed method was implemented on the MATLAB R2020b platform and compared with traditional geometric methods and numerical optimization methods. The experimental results show that the path generated by the proposed method has a length of 3.52 m, which is 15% shorter than the traditional geometric method and 2% shorter than the numerical optimization method, as shown in Figure 7. The time required to generate the path is 3.0 s, 40% shorter than the numerical optimization method, but slightly higher than the 0.8 s of the traditional geometric method, as shown in Figure 8. Additionally, the curvature fluctuation amplitude of the path is 0.08, which is 80% lower than that of the traditional geometric method and comparable to the 0.1 of the numerical optimization method, as shown in Figure 9. Overall, the proposed method significantly optimizes path length, curvature smoothness, and computational efficiency, with specific comparative results shown in Table 3.

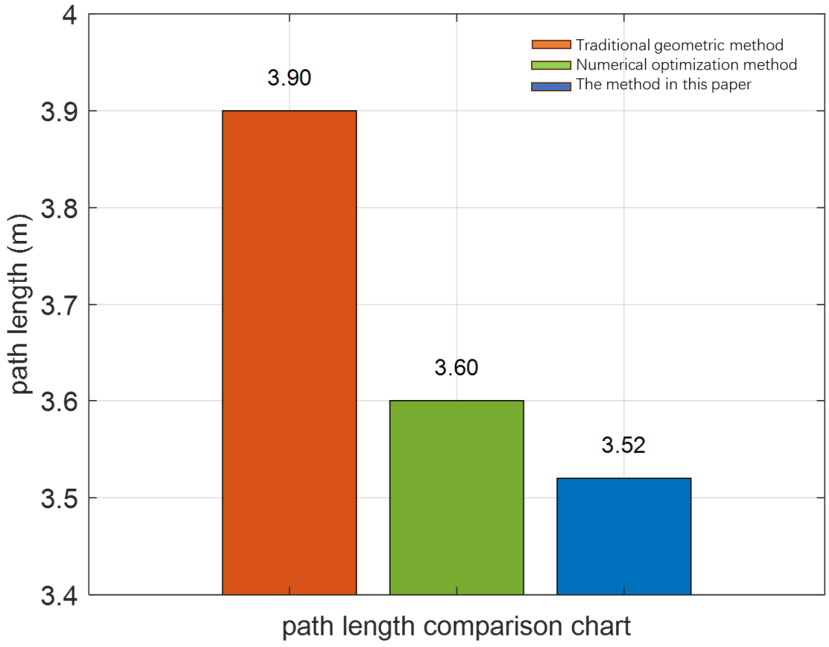


Figure 7. Comparison of parking path lengths generated by different methods.

In the context of this study, several simplifying assumptions were made to streamline the modeling and path planning process. For example, the vehicle was modeled as a rigid

body, and it was assumed that the wheels perform only rolling and steering motions. These simplifications reduce the model's complexity, allowing for more efficient path generation. However, it is important to note that the relationship between the steering angle and the turning of the vehicle's wheels is not strictly linear in reality. This could introduce some inaccuracies when applying the model to more complex or dynamic environments.

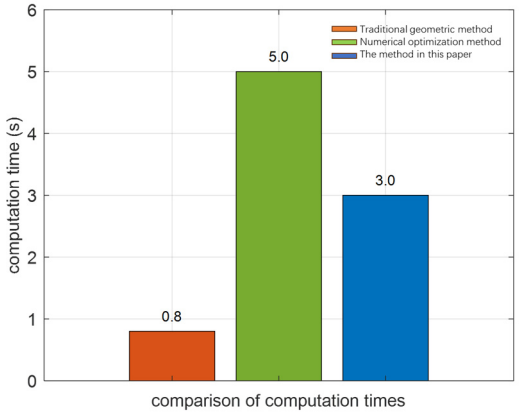


Figure 8. Comparison of computation times for parking paths generated by different methods.

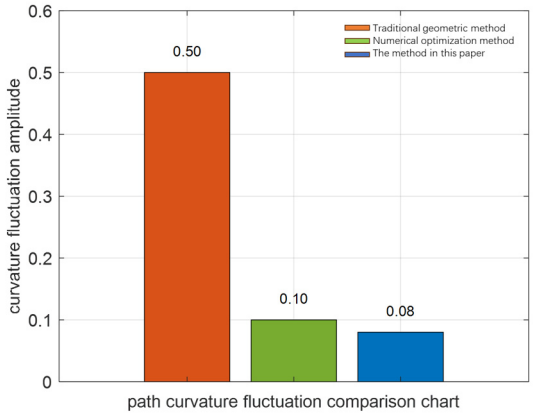


Figure 9. Comparison of curvature smoothness of parking paths generated by different methods.

Table 3. Performance Comparison of Different Path Planning Methods.

Method	Path Length (m)	Computation Time (s)	Curvature Fluctuation Amplitude (Maximum)
traditional geometric method	3.9	0.8	0.5
numerical optimization method	3.6	5.0	0.1
the method proposed in this paper	3.52	3.0	0.08

While these assumptions provided reasonably accurate predictions for the paths in this study, they may cause errors in more complex scenarios, such as when driving on low-traction surfaces or at larger steering angles. For instance, the assumption that lateral sliding of the wheels can be neglected during low-speed driving holds true for the parking scenarios in this study. However, in environments with lower traction or higher steering angles, tire slip may become more significant, potentially altering the trajectory of the vehicle.

To assess the impact of these simplifying assumptions, sensitivity analysis was conducted by varying friction coefficients and turning radii. The results showed minor deviations between the predicted paths and real-world data, particularly in conditions with low traction or large steering angles. While these deviations were minimal in the simulated

parking scenarios, they may become more noticeable in real-world applications. Future research will aim to incorporate the effects of tire slip and the nonlinear relationship between the steering angle and wheel rotation, which should improve the accuracy and broader applicability of the proposed method.

4.3. Vehicle Motion Trajectory Validation

The parking starting point coordinates (3.3, 3.6) were chosen for calculation. Using Matlab R2020b, the optimal combination of circular arcs and straight lines within the drivable area was obtained, as shown in Figure 10. The radius of the circular arc corresponding to the upper boundary of the drivable area is 2.8 m, while the radius corresponding to the lower boundary is 2.6 m. The optimal combination of circular arcs and straight lines has a circular arc radius of 2.7 m, situated in the middle of the drivable area.

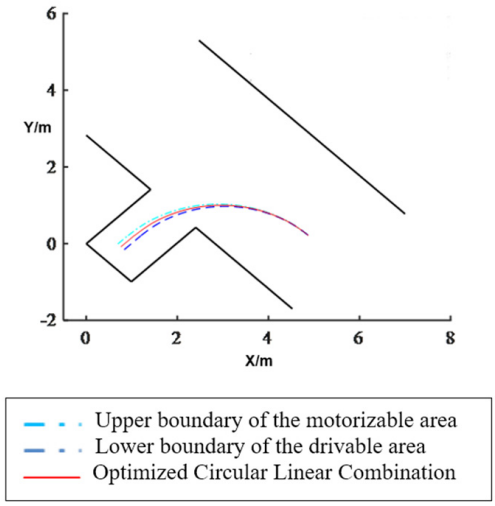


Figure 10. Drivable area and optimal circular arc and straight line combination for vertical parking.

As shown in Figure 11, the planned path curve is a smooth and continuous trajectory that connects the starting and ending points of the parking maneuver. The four body contour vertices of the target vehicle, labeled A, B, C, and D, meet the obstacle avoidance requirements, meaning each vertex can reach its corresponding endpoint without collision from its initial position. This indicates that the vertical parking path curve, planned using a fourth-degree polynomial, satisfies both position constraints and obstacle avoidance constraints.

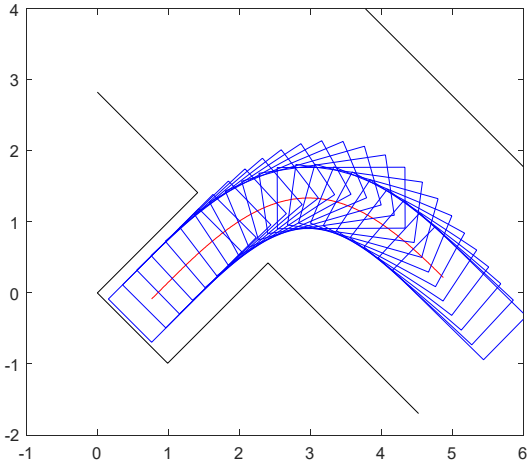


Figure 11. Rear axle center trajectory for vertical parking after smoothing.

As shown in Figure 12a, the derivative of the planned rear axle midpoint path curve at the parking starting point is −1, while at the parking endpoint, the derivative is 1. This indicates that at the parking starting point, the vehicle's body orientation is parallel to the horizontal direction of the parking space, whereas at the parking endpoint, the body orientation is perpendicular to the horizontal direction, thus satisfying the parking posture constraints. In Figure 12b, the planned rear axle midpoint path curvature is within the range of [−0.05406, 0.01887], which complies with the maximum allowable curvature requirements. Additionally, Figure 12c demonstrates that the equivalent front wheel steering angle variation during the parking process is smooth, without any abrupt changes. Furthermore, as depicted in Figure 12d, when the vehicle is moving at the maximum allowable parking speed, the variation in the equivalent front wheel steering angle rate along the planned path is steady.

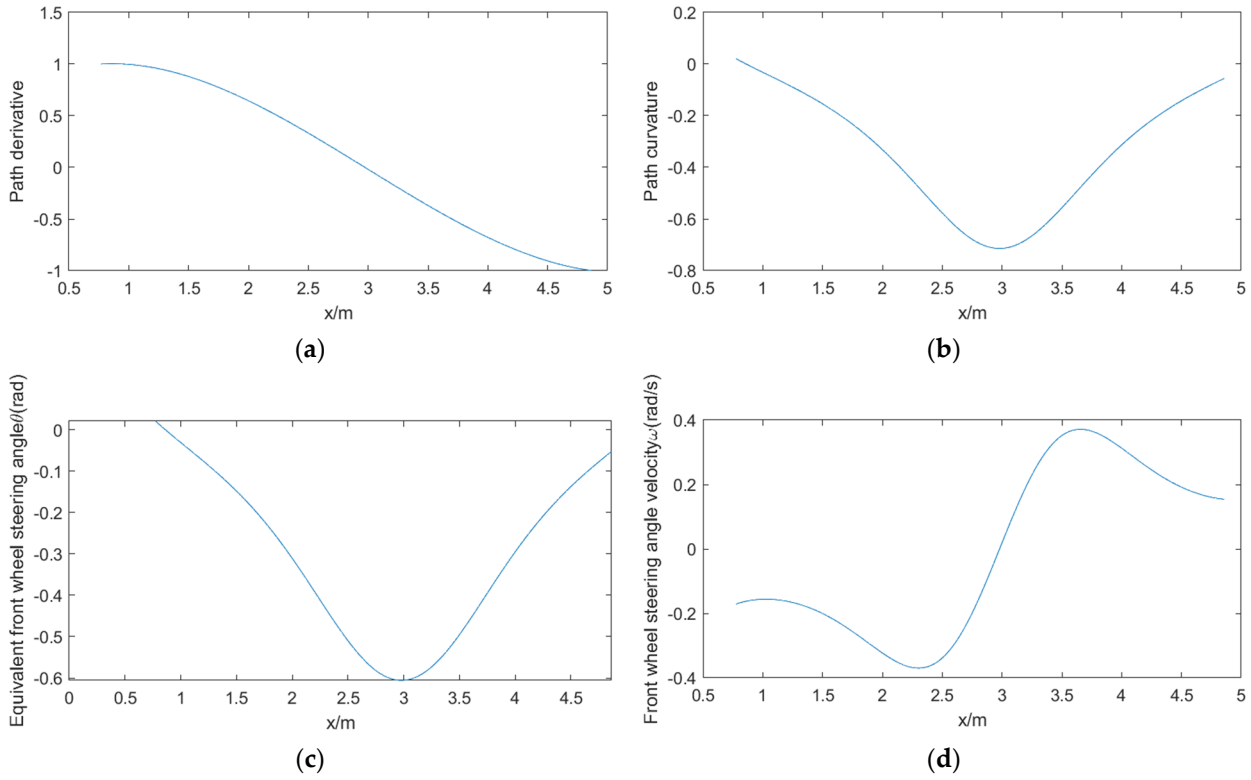
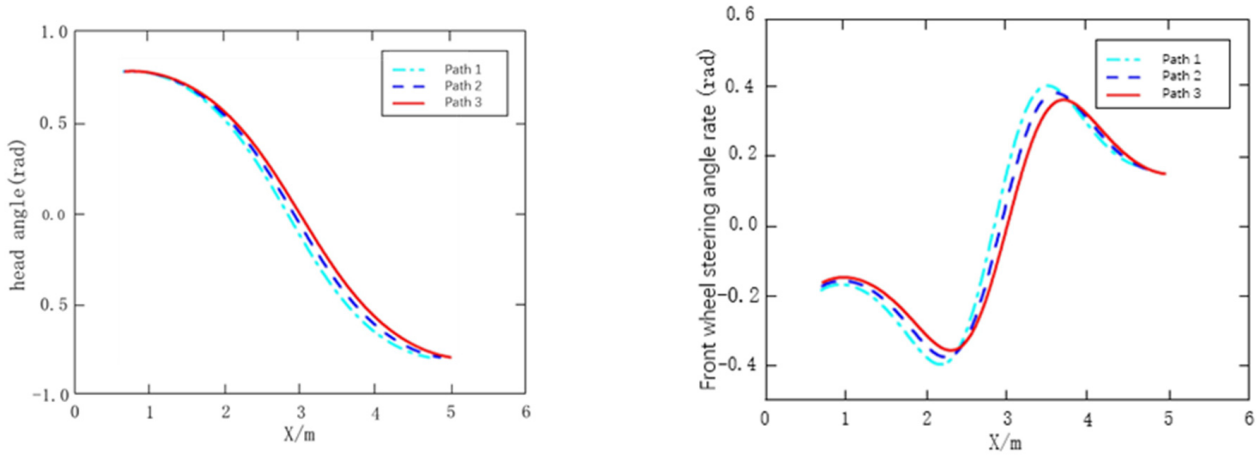


Figure 12. (**a**) The derivative of the vertical parking path curve; (**b**) the curvature of the vertical parking path curve; (**c**) the equivalent steering angle of the front wheels of the path curve; (**d**) the equivalent steering angle speed of the front wheels of the path curve.

To demonstrate the path planning performance for different parking start points, two additional sets of start coordinates, (3.2, 3.5) and (3.4, 3.7), were proportionally selected based on the initial start point (3.3, 3.6). A quartic polynomial was used for fitting. Due to the coordinate system being rotated counterclockwise by 45°, the heading angle value of 0.7 after rotation corresponds to a heading angle value of 0 before rotation. From Figure 13a, it can be observed that for the three different start points, the vehicle's heading angle at both the start and endpoints is 0, meeting the requirement for the vehicle's initial and final states to be parallel to the parking space. As shown in Figure 13b, the absolute value of the vehicle's maximum front wheel steering angle rate for all three paths is 0.403 rad/s, which satisfies the condition of being less than the vehicle's maximum front wheel steering angle rate of 0.478 rad/s, thus meeting the kinematic constraints.

In summary, the parking path curve based on fourth-degree polynomial planning exhibits excellent tracking performance while ensuring the stability and safety of the parking process under the constraints of vehicle environmental factors, posture, and kinematics.



(**a**) vehicle heading angle (**b**) front wheel steering angle rate

Figure 13. Simulation results of vertical parking path planning.

5. Conclusions

This research proposed a path planning method for vertical parking scenarios based on a combination of circular arcs, straight lines, and a multi-objective evaluation function, as illustrated in Figure 14. By analyzing the boundary limits of the vehicle's outer profile and the parking space, the upper and lower boundaries of the drivable area were determined through tangent points between circular arcs and straight lines. A multi-objective evaluation function was designed, based on path curvature, adjustable margin, and path length, to derive the optimal combination of circular arcs and straight lines within the drivable area. Subsequently, polynomial curves were employed to fit the optimal combination of circular arcs and straight lines, resulting in the generation of an optimal reference path. Simulation results indicate that the planned path satisfies the continuity of path curvature and adheres to the constraints of vehicle dynamics.

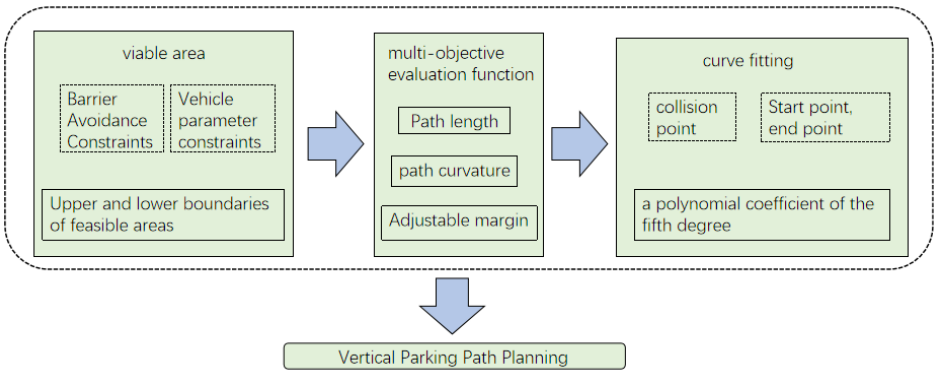


Figure 14. Vertical parking path planning framework diagram.

Author Contributions: Conceptualization, J.M. and Y.Q.; methodology, J.M.; software, J.M.; validation, J.M. and Y.Q.; formal analysis, J.M. All authors have read and agreed to the published version of the manuscript.

Funding: This research received no external funding.

Data Availability Statement: No new data were created or analyzed in this study. Data sharing is not applicable to this article.

Conflicts of Interest: The authors declare no conflicts of interest. The funders had no role in the design of the study; in the collection, analyses, or interpretation of data; in the writing of the manuscript; or in the decision to publish the results.

References

1. Zhang, Y.; Zhang, W.; Bi, J. Recent advances in driverless cars. *Recent Patents Mech. Eng.* **2017**, *10*, 30–38. [CrossRef]
2. Price-Robinson, K. Automated parking systems demystified: Answering the who, what, when, where, why, and how questions about this innovative technology. *Archit. Rec.* **2022**, 209.
3. Jang, C.; Kim, C.; Lee, S.; Kim, S.; Lee, S.; Sunwoo, M. Re-plannable automated parking system with a standalone around-view monitor for narrow parking lots. *IEEE Trans. Intell. Transp. Syst.* **2020**, *21*, 777–790. [CrossRef]
4. Idris, M.Y.I.; Leng, Y.Y.; Tamil, E.M.; Noor, N.M.; Razak, Z. Car park system: A review of smart parking systems and their technology. *Inf. Technol. J.* **2009**, *8*, 101–113. [CrossRef]
5. Li, B.; Acarman, T.; Zhang, Y.; Ouyang, Y.; Yaman, C.; Kong, Q.; Zhong, X.; Peng, X. Optimization-based trajectory planning for autonomous parking with irregularly placed obstacles: A lightweight iterative framework. *IEEE Trans. Intell. Transp. Syst.* **2022**, *23*, 11970–11981. [CrossRef]
6. Chen, X.; Li, B.; Fan, L.; Zhang, Y. A review of motion planning methods for autonomous parking. *Control. Inf. Technol.* **2024**, 1–13.
7. Gómez-Bravo, F.; Cuesta, F.; Ollero, A.; Viguria, A. Continuous curvature path generation based on β-spline curves for parking manoeuvres. *Robot. Auton. Syst.* **2008**, *56*, 360–372. [CrossRef]
8. Wang, H.; Li, Y.; Liu, J. Motion planning for automated parking systems: A survey. *Int. J. Autom. Comput.* **2020**, *17*, 211–224.
9. Zhang, X.; Yang, Z.; Guo, X. Research on motion planning for autonomous parking using a modified RRT algorithm. *IEEE Access* **2021**, *9*, 4583–4594.
10. Sun, Z.; Xu, W.; Wang, F. Path planning for autonomous parking using an improved particle swarm optimization algorithm. *J. Intell. Robot. Syst.* **2019**, *95*, 841–852.
11. Chen, M.; Liu, H.; Li, T. Optimal path planning for autonomous parking with dynamic obstacles. *IEEE Trans. Veh. Technol.* **2022**, *71*, 171–182.
12. Zhang, J.; Wang, Y.; Li, Z. A new approach to autonomous parking: Combining machine learning and traditional algorithms. *IEEE Trans. Autom. Sci. Eng.* **2020**, *17*, 150–160.
13. Li, X.; Zhang, Q.; Chen, Z. A hierarchical trajectory planning method for autonomous parking. *J. Field Robot.* **2021**, *38*, 778–791.
14. Zhao, Y.; Tang, C.; Liu, Q. A deep reinforcement learning approach for autonomous parking system. *IEEE Access* **2021**, *9*, 4562–4573.
15. Zhang, M.; Cheng, W.; Huang, Z. Path optimization for autonomous parking based on the A* algorithm. *J. Intell. Robot. Syst.* **2018**, *91*, 271–285.
16. Wang, Z.; Zhang, Y.; Li, T. Adaptive motion planning for autonomous parking using a genetic algorithm. *IEEE Trans. Ind. Electron.* **2021**, *68*, 12349–12358.
17. Li, Y.; Chen, S.; Liu, W. Autonomous parking using a hybrid trajectory planning algorithm. *IEEE Trans. Autom. Sci. Eng.* **2020**, *17*, 2345–2356.
18. Zhang, T.; Xu, D.; Ma, C. Real-time path planning for autonomous vehicles in parking lot environments. *IEEE Trans. Veh. Technol.* **2020**, *69*, 6657–6668.
19. Liu, X.; Guo, S.; Li, P. Optimization-based parking path planning for autonomous vehicles. *IEEE Trans. Intell. Transp. Syst.* **2022**, *23*, 11822–11834.
20. Wang, Z.; Song, Y.; Zheng, H. A model-based motion planning approach for autonomous parking. *IEEE Trans. Ind. Electron.* **2020**, *67*, 7712–7721.
21. Lee, J.; Kim, D.; Choi, S. Autonomous parking with trajectory optimization based on quadratic programming. *IEEE Trans. Veh. Technol.* **2021**, *70*, 3881–3890.
22. Chen, X.; Song, H.; Zhang, Y. A fast and reliable motion planning method for autonomous parking. *J. Field Robot.* **2020**, *37*, 49–59.
23. Li, X.; Wang, L.; Yang, L. A novel motion planning approach for autonomous parking with real-time obstacle detection. *Int. J. Autom. Comput.* **2019**, *16*, 491–502.
24. Kumar, V.; Li, S.; Brown, D. Autonomous parking systems: A review of algorithms and technologies. *Automot. Eng.* **2019**, *42*, 123–135.
25. Li, J. *Research on Path Planning and Tracking Algorithms for Autonomous Parking System Based on Four-Wheel Steering*; Jilin University: Changchun, China, 2023.

26. *ISO 16787*; Intelligent Transport Systems—Assisted Parking System (APS)—Performance requirements and test procedures. International Organization for Standardization (ISO): Geneva, Switzerland, 2016.
27. *GB/T 41630-2022*; Intelligent Parking Assist System Performance Requirements and Test Methods. Standardization Administration of China (SAC): Beijing, China, 2023.

Disclaimer/Publisher's Note: The statements, opinions and data contained in all publications are solely those of the individual author(s) and contributor(s) and not of MDPI and/or the editor(s). MDPI and/or the editor(s) disclaim responsibility for any injury to people or property resulting from any ideas, methods, instructions or products referred to in the content.